Numerical Simulation of the Hydrodynamic Ship Performance

Adham S. Bekhit(✉) and Adrian Lungu

"Dunarea de Jos", University of Galati, Galati, Romania
{adham.bekhit,adrian.lungu}@ugal.ro

Abstract. The study provides a numerical investigation of the ship hull performance for the Japan Bulk Carrier (JBC hereafter). The study includes computations for the ship resistance, trim and sinkage, free-surface elevation and wake flow for both, the bare hull and for the ship equipped with an energy saving device. The aim of this study is to investigate the efficiency and accuracy of the Computational Fluid Dynamics (CFD hereafter) technique as an effective and reliable tool to predict the ship hull performance in the early design stages and to highlight the effect of using an Energy Saving Device (ESD hereafter) on the reduction of total ship resistance. The computations are performed by using the ISIS-CFD solver of the commercial software FINE^{TM}/Marine. The flow solution is obtained by solving numerically the Reynolds-averaged Navier-Stokes equations in which the turbulence is modelled either by k-ω Shear Stress Transport (SST) or by the EASM models. The validation of the computed solutions is based on various comparisons with the experimental data provided in the Tokyo workshop 2015.

Keywords: Free-surface flow · JBC · Numerical simulation · RANSE
Ship resistance · Turbulence modelling

1 Introduction

Since the widespread use of propeller driven steel ships in the past century, there has been a sustained but sometimes unsteady effort to identify technologies which offer to improve the energy efficiency of marine propulsion. It has already been proved that sixteen of the world's largest ships are still producing as much sulphur pollution as all the cars of the planet. So, what's the key to 'green shipping'? How do we reduce fuel consumption & emissions? Here we share the top 5 technologies that the largest shipping companies across the globe are using to dramatically reduce the environmental impact of their operations and, subsequently, boost profits. The International Maritime Organization (IMO hereafter) third greenhouse gas emission study in 2014 concluded that the maritime transport emitted 938 million tons of CO_2 in 2012, representing 3.1% of the world's total emissions, and that the total fuel consumption of shipping is dominated by three ship types: oil tankers, container ships and bulk carriers. Consistently for all ship types, the main engines are the dominant fuel consumers, and according to the IMO assessment of future scenarios, without intervention, maritime emissions could rise by 50–250% by 2050 compared to 2011.

T. Kováčiková et al. (Eds.): INTSYS 2017, LNICST 222, pp. 120–129, 2018.
https://doi.org/10.1007/978-3-319-93710-6_14

As each ship is different and each technology has a specific design point, clearly not all technologies will suit each ship. The current emerging requirement for improved energy efficiency has three main drivers: the increasing cost of energy, its impact on the environment and to a lesser extent, energy security. The paper presents an assessment of an emerging solution in the context of a bulk carrier. Since 1999, a series of studies for a wide range of studies in the propulsion efficiency and energy conservation has continuously been done. An impressive database of over 100 technologies of varying degree of maturity has been built for identifying the most effective means in terms of fuel saving and emission reduction.

In 2013 the American Bureau of Shipping (ABS hereafter) released an Advisory has compiled the worldwide data to provide useful information on the status and the current state of ship energy efficiency measures. It provides guidance to owners and operators on the wide range of options being promoted to improve vessel efficiency, reduce fuel consumption and lower emissions. Included is background information, descriptions of the technologies, explanations of key issues, general pros/cons of each measure and limits of applicability or effectiveness, as well as practical issues related to implementation. The ABS document is structured in five sections: (i) hull form optimization, (ii) energy-saving devices, (iii) structural optimization and light weight construction, (iv) machinery technology, (v) fuel efficiency of ships in service.

The aim of the present paper is to present a study related to the second problem listed above, based on the fact that a major challenge for this engineering field is to find a quick, reliable and cheap tool to enhance the efficiency, economy and safety of a ship, by making use of the CFD tools. The large development of the CFD in the past decades accompanied by the development of the hardware made it possible to think of simulation based design as a new technique aimed at replacing the out-of-fashioned ones based on tank testing and sea-trials.

In 2015 and in the scope of the seventh Workshop on CFD in ship hydrodynamics, the JBC hull, which is a capesize bulk carrier equipped with a duct works as an energy saving device was proposed as a benchmark for CFD investigations. The National Maritime Research Institute (NMRI hereafter), Yokohama National University and Ship Building Research Centre of Japan were jointly involved in the design of the ship hull, the duct and the rudder. Towing tank experiments were planned at NMRI, SRC and Osaka University, which included resistance and self-propulsion tests as well as PIV measurements of stern flow fields [1]. The purpose of designing the JBC was to provide a new and challenging hull with energy saving device to assess the state of the art from the previous workshops and to investigate the accuracy of CFD methods for predicting new concept designs. Following the main concept of the workshop, this numerical investigation is carried out to investigate the accuracy of CFD as a reliable tool for predicting ship hull performance in different ship related problems.

The numerical simulation includes computations for ship resistance with motion calculations for two degrees of freedom including sinkage and trim. Besides, computations for free-surface flow and wake flow calculations in the stern of the ship. These previously mentioned computations are to be covered in the first part of this paper providing results for ship with and without the ESD. The results will be provided for two different turbulence modelling; Menter's k-ω SST [2] and EASM models [3] to

find out the optimum model to predict the most accurate results. Validation of results is based on the tank test results provided by NMRI [4].

2 Computational Conditions

The computations are performed using ISIS-CFD solver available by Fine^{TM}/Marine commercial software provided by NUMECA. The solver is based on the quasi-steady finite volume method to provide a spatial discretization for the governing equation to solve the Reynolds averaged Navier-Stokes equations in a global approach. Closure to the turbulence is done by using the k-ω SST and EASM models. The free-surface topology is computed based on the volume of fluid method, which captures the free-surface location within an air-water interface. The interface capturing method used in the present study is based on a compressive advection discretization scheme which is applied to the volume fraction equation. Discretization in time is made using a steady time marching quasi-static approach. The computational domain is fully rectangular and it is defined in such a way to take advantage of the symmetry of the hull.

The computational domain extends from $1.0L_{pp}$ at the upstream to $3.0L_{pp}$ at the downstream, while the lateral side is located at $2.0L_{pp}$ from the symmetry plane. Here L_{pp} stands for the length between perpendiculars. The bottom is located at $1.5L_{pp}$ and the top is placed at $0.5L_{pp}$ in respect to the undisturbed free-surface. The boundary conditions imposed to solve the partial differential set of equations that describes the flow are based on either Dirichlet or Newman formulations for the pressure, velocity components and turbulence characteristics. The symmetry condition is applied on the ship centreline, whereas a no-slip boundary condition is imposed on the solid boundaries with a wall function defined by $y^+ = 31.0$.

The computational grid is generated by using the HEXPRESS automatic grid generator. Unstructured grids with hexahedral elements are created by imposing similar restrictions for the discretisation. The integration in time is done based on second order convergence criteria using combined upwind scheme and cantered scheme. The flow is accelerated for 10 s using a quasi-static approach which helps reducing the need of using a very small time-step. The simulation time is 30 s with a time step ranging from 0.01 to 0.001 depending on the grid cell size.

3 Results and Discussions

Any possibly complex geometry of both the free surface and hull as well as the accurate approximation of surface tension forces may require a sufficiently fine grid in a neighborhood of the significant boundaries. The use of uniform grids becomes prohibitively expensive, especially in 3D simulations. Under such circumstances locally refined meshes often need considerably less computational resources. However, such meshes have to be dynamically refined and coarsened if the free surface evolves. Since the re-meshing is, in general, CPU time and memory expensive, the simulations reported in here were performed without taking advantage of the refinement.

The present study is performed for the model scale of the given ship with a length between perpendiculars L_{pp} = 7.0 m, towed at a velocity of 1.179 m/s to which the corresponding Froude number is 0.142, whereas the Reynolds number is 7.46E+06. The JBC ship model is depicted in Fig. 1 which shows the ship hull with and without ESD. The only difference between the two hulls consists in the addition of the duct having a circular shape with a NACA4420 foil section that has an opening angle of 20 degrees. The diameter of the duct is 55% of the propeller diameter and the chord length is 30% of the same diameter. The duct is connected to the hull by means of a strut profiled hydrodynamically.

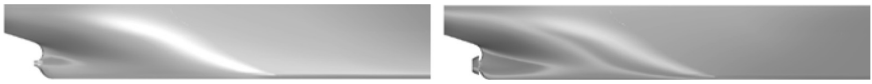

Fig. 1. JBC ship model stern shape without ESD (left) and with ESD (right).

For the verification and validation purposes, two grid convergence tests are performed on four different meshes. They have successively been generated for both cases considered, i.e. with and without ESD with a refinement ratio of about 1.7. For the sake of numerical consistency, the turbulence model and the time step value are kept unchanged. Table 1 summarizes the mesh density for the four meshes generated for the JBC hull with and without ESD, where Grid 1 refers to the finest mesh and the Grid 4 refers to the coarsest one.

Table 1. Number of grid cells for ship model with and without ESD.

Grid Size	Numerical Model	
	JBC w/o ESD	JBC with ESD
Grid 1	7.462 M	9.670 M
Grid 2	4.587 M	5.881 M
Grid 3	2.602 M	3.583 M
Grid 4	1.506 M	2.107 M

A sample of the computational grid on which the simulations reported here is shown in Fig. 2, which depicts the finest generated mesh drawn only at the extremities of the ship for the hull appended with the ESD.

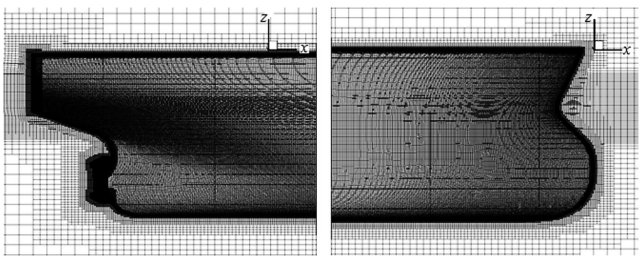

Fig. 2. Computational grid at the extremities of the JBC model equipped with ESD.

In most of the computations considered in the present paper, the convergence of the resistance has been reached after about 18 s of physical time, while the convergence of motion has been reached after more than 20 s, depending on the mesh size. Several sets of computations are performed in an attempt of clarifying the details concerning not only the ship resistance, but also the sinkage and trim motions, the free-surface geometry and the intrinsic issues of the local flow at the stern of the ship. In the followings, the main issues of their dominant characteristics will be successively presented and discussed.

3.1 Ship Resistance Problem

Table 2 summarizes the sixteen sets of the computed solutions tabulated as a function of the grid density and with respect to the turbulence model used in the present research. It is clearly noticed that the EASM gives a higher level of accuracy with an error range between1.36% and 2.57% for ship without ESD, while for ship with ESD the error range was between 0.45% and 4.11%. On the other side, the k-ω turbulence model showed a relatively lower level of accuracy compared to EASM which ranged between 2.8% and 6.42% for the ship without ESD and ranged between 3.1% and 6.8% for the ship equipped with the ESD. The error range can be considered as being acceptable especially for finer meshes, therefore the computed resistance compared to the corresponding measured one prove to be close enough, a fact that proves the overall accuracy of the solver.

Table 2. Resistance results for ship with and without ESD for the k-ω and EASM turbulence models.

EFD	Numerical Model			
	JBC w/o ESD C_T = 4.289		JBC with ESD C_T = 4.263	
Turbulence model	EASM	k-ω	EASM	k-ω
Grid 1 Error	4.231 1.36%	4.169 2.8%	4.282 0.45%	4.131 3.1%
Grid 2 Error	4.227 1.45%	4.112 4.13%	4.227 0.84%	4.097 3.9%
Grid 3 Error	4.224 1.52%	4.087 4.71%	4.206 1.1%	4.055 4.8%
Grid 4 Error	4.179 2.57%	4.014 6.42%	4.088 4.11%	3.97 6.8%

In the followings, a comparison is proposed to investigate the effect of the ESD on the total resistance of the ship. The numerical solutions are compared in terms of the total resistance R_T of the ship with and without ESD for different operating speeds, as Fig. 3 bears out. The comparison reveals a favourable reduction in the total resistance with about 1.46% due to the addition of duct, a fact which eventually contribute to a power reduction, therefore to an increase of the efficiency.

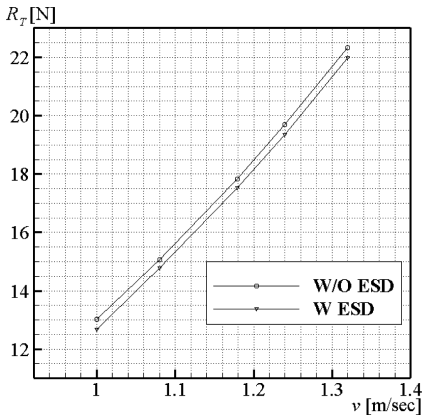

Fig. 3. Comparisons between the total resistance curves computed for the two considered hulls at different velocities.

The computed sinkage and trim shows a good agreement with the experimental data, regardless of the turbulence model used. For instance, the sinkage value computed for the ship without the ESD at T = 30 s was –0.0872 with an error level of 1.4% compared to the measured value of –0.086 as a percentage of L_{PP}, where the negative value shows the direction considering upward positive. In case of the ship equipped with the ESD the value computed for sinkage was –0.877 with an error of 3.18% compared to the measured value of 0.085. The error ranged up to 6.23% in the case of the ship appended with the ESD as the highest value of error for all the computations reported in here. The reason for such a level of error resides apparently in the imbalance between the cells sizes measured in the free-surface vicinity at the extremities of the ship. The trim was computed for the ship model without ESD at T = 30 s as –0.178 with an error 1.12% compared to the measured value of -0.18, while the negative value corresponds to the condition bow up is positive. The computed trim for the ship with the ESD was 0.175 with an error 3.74% compared to the corresponding computed value of –0.182 percentage of L_{PP}. The highest level of error was found for the case of the ship equipped with the ESD, for which the difference between the computation and the experiment was 5.32%.

3.2 Free-Surface Topology

One of the most important issues in ship hydrodynamics is the free-surface geometry since it influences directly the wetted area of the ship based on which the ship resistance is calculated. Besides, errors in computed wave profiles may determine misleading judgements concerning other phenomena related to the flow, such as the wave breaking, trim and sinkage, stability and so on. That is why all the theoretical approaches focus on the accuracy the location of the water surface is computed with. For validation reasons, a comparison of free-surface results for JBC is proposed in the followings only for the ship without ESD case as the experimental data are only provided for this case. The comparison between the numerical solution computed at

T = 30 depicted in Fig. 4 and the corresponding experiment of Hirata [4] shows a satisfactory overall agreement. Nevertheless, the wave height is slightly over predicted in the fore part with approximate error of 2.52%. This may be attributable either to the radiation induced by the numerical scheme, towards the upstream, or to the lack of ability in the treatment of the sub-breaking regime, which always occurs in the area where the bow intersects the water surface. It has already been proven that not only the necklace vortices generation, but also their maintenance require energy consumption, therefore the wave crest may get smaller than expected. So if the numerical scheme fails to accurately capture those heavy-turbulent structures, the height of the bow crest may result larger, as it happens in the present research.

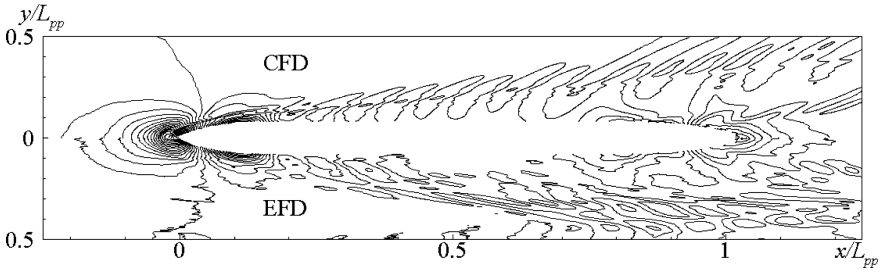

Fig. 4. Comparison between the free-surface shape computed at T = 30 s and measured [4].

It is worth mentioning that the computed free-surface reveals not only a slight phase shift in respect to the measured elevation near the aft shoulder, but also a difference in the height of the crest. Seemingly this fact can be related to the insufficient number of cells used there, a fact which possibly suggest a higher grid refinement in that area. Obviously, this fact may be easily in Fig. 5 which bears out a comparison the computed and measured [4] wave profiles drawn along the ship hull.

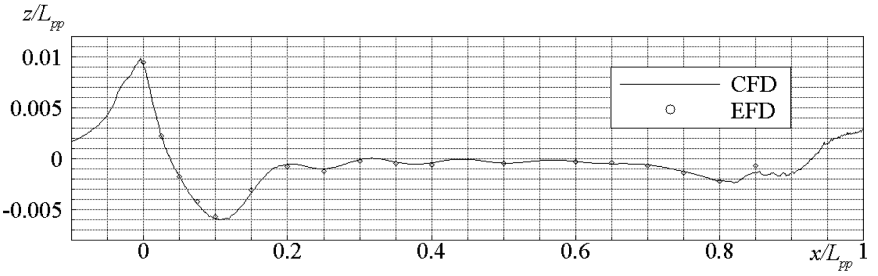

Fig. 5. Comparison between the wave profiles along the hull computed at T = 30 s and measured in the towing tank [4].

Similarly, comparisons between the wave cuts made at a distance of y/L_{PP} = 0.1043 and of y/L_{PP} = 0.19 are brought into focus in Figs. 6 and 7, respectively. The comparisons reveal a reasonable agreement of the computed solution with

the experimental data [4], although the abovementioned over prediction in the fore area is still present. Moreover, the same under prediction of the heights of the crests downstream of the ship still persist, a fact that may suggest once again the need of a special grid refinement in that area on the free-surface. Since it was already proved in the literature that a larger grid size always induces a numerical dissipation, the authors believe that this is the reason for having such differences in the two sets of data compared in the aforementioned figures.

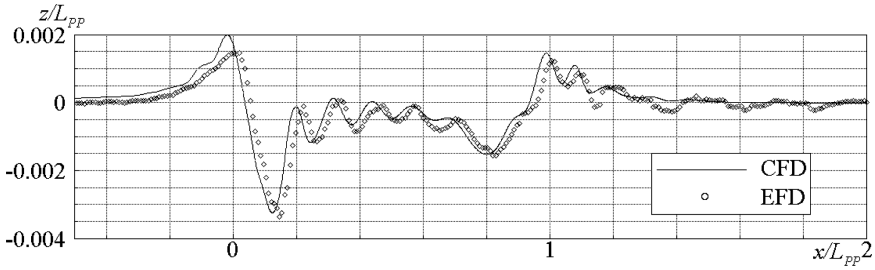

Fig. 6. Comparison of the wave cuts at $y/L_{PP} = 0.1043$ computed at T = 30 s and measured [4].

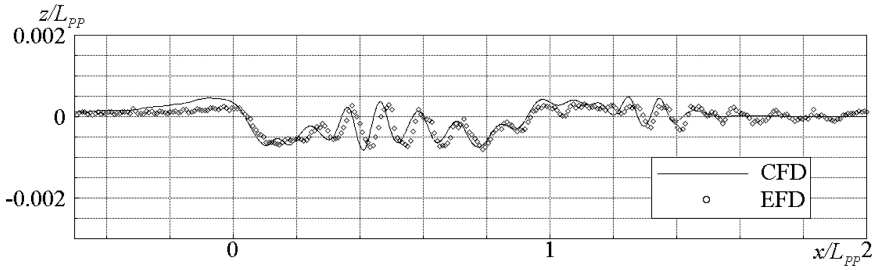

Fig. 7. Comparison of the wave cuts at $y/L_{PP} = 0.19$ computed at T = 30 s and measured [4].

3.3 Local Flow Features

The flow at the model scale around the JBC hull is characterized by the gradual development of an intense stern bilge vortex which leads to a significant distortion of the axial velocity iso-contours at the propeller plane. This distortion is due to the transport of low momentum fluid from the vicinity of the hull to the center of the flow field under the action of an intense longitudinal vortex. Under the main vortex, one can guess the existence of a secondary counter-rotating vortex close to the vertical plane of symmetry. This leads to the so-called hook-shape of the iso-wakes which is clearly visible in the towing tank and wind tunnel experiments. Doubtless, significant improvements in the after-body flow were reported in the past decade and the quality of the vortical and turbulent structures reported are by far better than those before. The improved predictions are due to reduction in modelling and discretization errors. The increased computational power nowadays allows simulations on finer grids, a fact that helps in reducing discretization errors, therefore in the prediction of vortical and

turbulence structures. The wide range of turbulence models including the unsteady RANS with isotropic and anisotropic turbulence models, hybrid RANS/LES with detached eddy simulation (DES) or Large Eddy Simulation (LES) used in the community may raise a doubt upon the balance between the accuracy and the costs implied by a numerical simulation. Under these circumstances, being restricted at a limited number of 120 processors, the authors of the present paper employed only the k-ω and EASM models, which are significantly cheaper in terms of the computational resources. Obviously, both of them proved not only a proper prediction of bilge vortex development, but also a satisfactory capability in capturing the hook shaped distribution of the streamwise velocity in the stern region. However, for coarser meshes the solution seems to be under predicted, as expected. This problem does not exist on the finer meshes where the solution agrees with the experimental data [4].

For validation reasons, three locations denoted by S2, S4 and S7 same as those in which the LDV measurements were done [4–6] in the stern region. S2 is located before the duct at a distance of 262.5 mm from the aft perpendicular, S4 is between duct and propeller being placed at 110 mm from aft perpendicular, whereas S7 is placed in the origin of the Cartesian system of coordinates. In the followings several comparisons between the computed solution and the experimental data will be proposed as an attempt in providing the robustness of the numerical approach described in the present paper. All the comparisons refer to the flow simulations around the ship hull equipped with the ESD. Figure 8 shows a comparison of the streamwise velocity field computed in the S2 station by using the EASM turbulence model for the finest mesh at T = 30 s compared with the experimental data [4]. The good agreement between the two may emphasize the solver capability to reproduce the complexity of the flow structure in that area, a fact which is crucially important for a proper design of the propeller working in the ship wake.

Similarly, for the measuring stations S4 and S7, the comparisons between computed velocity contours in the x-direction and the experimental data reveals again a good resemblance, as Figs. 9 and 10 prove. Finally, the comparison between the numerical solutions computed by using the EASM and k-ω SST turbulence models

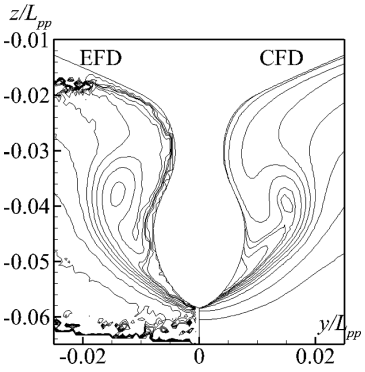

Fig. 8. Comparison between the streamwise velocity contours measured and computed at T = 30 s at 262.5 mm in front of the A.P.

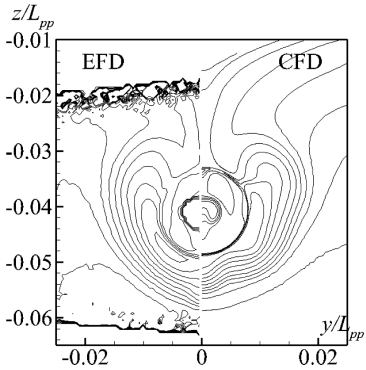

Fig. 9. Comparison between the streamwise velocity contours measured and computed at T = 30 s at 110 mm in front of the A.P.

proposed in Fig. 11, proves that the EASM seems to be more accurate than the k-ω SST model, which slightly under predicts the velocity contours.

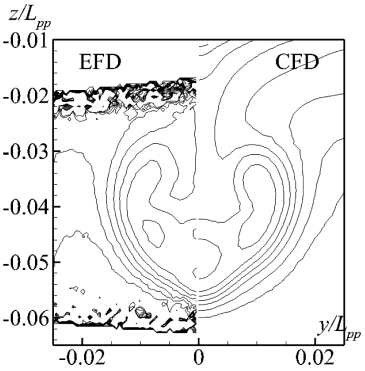

Fig. 10. Comparison between the streamwise velocity contours measured and computed at T = 30 s in the A.P.

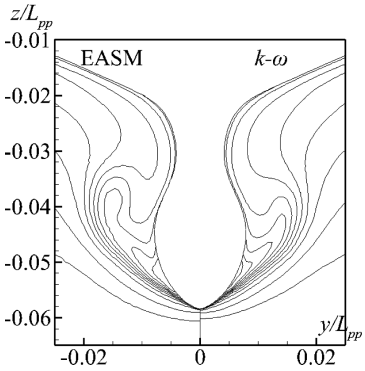

Fig. 11. Comparison between the streamwise velocity contours computed at T = 30 s at S2 by using the EASM and k-ω SST models.

4 Concluding Remarks

Comprehensive numerical investigations performed on the JBC benchmark model for different ship hydrodynamics related problems such as: resistance, free-surface flow or sinkage and trim estimation. Several introspections into the local flow features are proposed for getting a grasp of understanding of the complexity of the flow mechanism. A validation of the numerical solution performed based on the comparisons with the available tank test measurements [4] proves a satisfactory agreement between the computed results and the corresponding measured data, a fact that may sustain in the future the efforts paid for the development of robust numerical tools as an alternate design method. The numerical investigation on the effect of the ESD on the total ship resistance proved to be useful. The ESD use leads to a 1.46% reduction of the total resistance.

References

1. NMRI, Tokyo, A Workshop on CFD in Ship Hydrodynamics (2015). http://www.t2015.nmri.go.jp/jbc.html
2. Menter, F.R.: Two-equation eddy-viscosity turbulence models for engineering applications. AIAA J. **32**(8), 1598–1605 (1994)
3. Gatski, T.B., Speziale, C.G.: On explicit algebraic stress models for complex turbulent flows. J. Fluid Mech. **254**, 59–78 (1993)
4. Hirata, N. (2015). http://www.t2015.nmri.go.jp/Presentations/Day1-AM2-JBC-TestData1-Hirata.pdf
5. Larsson, L.: Resistance, Sinkage, Trim and Wave Pattern Review, Tokyo (2015). http://www.t2015.nmri.go.jp/Presentations/Day1-AM4-JBC-Resist_etc-Larsson.pdf
6. Vissoneau, M. (2015). http://www.t2015.nmri.go.jp/Presentations/Day1-PM1-JBC-LocalFlow-Visonneau.pdf